J. Fluid Mech. (1985), *vol.* 152, *pp.* 145–161
Printed in Great Britain

Bifurcation in steady laminar mixed convection flow in horizontal ducts

By K. NANDAKUMAR, JACOB H. MASLIYAH AND HIN-SUM LAW

Department of Chemical Engineering, University of Alberta, Edmonton, T6G 2G6, Canada

(Received 18 March 1984 and in revised form 26 June 1984)

The fully developed laminar mixed-convection flow in horizontal ducts of rectangular, circular and semicircular cross-sections has been studied using a numerical model of the governing equations of motion, subject to the Boussinesq approximation and an axially uniform heat-flux condition. Dual solutions with a two- and a four-vortex flow pattern have been observed in all cases. The rectangular geometry, with its aspect ratio and Grashof number as parameters, is posed as a two-parameter problem. In this parameter-space, the critical points where the transition between the two- and the four-vortex pattern occur, follow a tilted cusp. This is akin to the phenomenon in the Taylor problem which has been thoroughly investigated by Benjamin and co-workers in a general study of bifurcation phenomena for viscous flow problems. The bifurcation phenomenon in circular ducts, which is essentially a one-parameter problem, has features similar to that observed for the Dean problem, by Nandakumar and Masliyah.

1. Introduction

The problem of free and mixed convection in enclosures has been extensively studied. Jaluria (1980) presents a good introduction to many facets of this problem. Subject to a wide variety of thermal boundary conditions, the problem of mixed convection in ducts has been discussed in numerous papers. Among the theoretical works, Morton (1959), Faris & Viskanta (1969) and Iqbal & Stachiewicz (1966, 1967) have all used perturbation approach. Cheng & Hwang (1969), Hwang & Cheng (1970), Newell & Bergles (1970) and Patankar, Ramadhyani & Sparrow (1978) have developed numerical solutions using finite-difference methods. Mori *et al.* (1966), McComas & Eckert (1966), Shannon & Depew (1968), Bergles & Simonds (1971), Kato *et al.* (1982) and a number of others have studied the problem experimentally.

The specific problem that we wish to study is that of fully developed laminar mixed convection flow in horizontal rectangular, circular and semicircular straight ducts subject to the thermal conditions of axially uniform wall heat flux and peripherally uniform wall temperature.

The equations governing the mixed convection flow problem are very similar to those of laminar flow in helical tubes (the Dean problem) and to Couette flow between rotating cylinders (the Taylor problem). Flow bifurcation in the Taylor problem is known to exist. This problem has been examined in great detail by Benjamin and co-workers (Benjamin 1978*a*,*b*; Benjamin & Mullin 1981, 1982; Mullin 1982) in a general study of bifurcation phenomena in viscous flow problems. Some of their essential findings for the Taylor problem areas follow: (i) it can exhibit profuse multiplicity; (ii) certain anomalous and asymmetric modes of flow behaviour are

possible; (iii) the end effects are important, no matter how large the aspect ratio is. More recently Cliffe (1983) has computed some of the flow mutations predicted and observed by Benjamin and co-workers.

Studies on bifurcation phenomena in the Dean problem have been more limited in scope. Nevertheless, dual solutions have been observed in both experimental and numerical studies by Cheng, Nakayama & Akiyama (1977), Masliyah (1980), Nandakumar & Masliyah (1982) and Dennis & Ng (1982).

A number of investigators have perceived a close similarity between the Dean problem and the mixed convection problem. As pointed out already, the mixed convection problem has been examined by a number of investigators. Yet there is no record of flow bifurcation for this problem. The question that needs to be answered then is whether, on increasing the flow parameter (Grashof number) sufficiently, the mixed convection flow bifurcates as well. In this communication we examine this possibility for several duct geometries. An affirmative answer will lend support to the perception that the mixed convection problem can also exhibit a number of features observed for the Taylor problem. However, the establishment of profuse multiplicity or anomalous mode behaviour would require either careful experimentation or the use of advanced numerical methods such as the arc length continuation method of Keller (1977). We do not address this problem in its full complexity at present, but restrict it to a symmetric flow, and the transition between a two- and a four-vortex pattern for several geometries.

2. Governing equations

Two coordinate systems are employed. A Cartesian system of coordinates is used for the straight rectangular ducts and a cylindrical bipolar coordinate system is used for the case of circular and semicircular straight ducts. The latter coordinate system permits a smooth variation in the geometrical shape from a full circle to a semicircle. Such a facility is essential if the flow pattern is not to be perturbed significantly by changes in geometrical shape. The bipolar system of coordinates was used successfully by Nandakumar & Masliyah (1982) for studying the bifurcation phenomenon in the Dean problem.

The formulation of the buoyancy effects was made using the Boussinesq approximation to account for the density variation insofar as it affects the body force term, but otherwise the density is assumed to be constant. Making use of Boussinesq approximation, the Navier–Stokes equation becomes

$$\boldsymbol{v}'\cdot\boldsymbol{\nabla}\boldsymbol{v}'-\nu\boldsymbol{\nabla}^2\boldsymbol{v}'=-\frac{\boldsymbol{\nabla}'p^*}{\rho}+\beta\boldsymbol{g}(T_{\mathrm{w}}-T), \tag{1}$$

where p^* is the dynamic pressure, $\boldsymbol{g}$ is the gravitational force, β is the coefficient of thermal expansion and T_{w} is the duct wall temperature and it is given as a function of z. The condition of axially uniform flux implies that both the wall temperature and the bulk fluid temperature vary linearly with the axial position. The z-direction of (1) gives the axial velocity equation. The prime denotes dimensional quantities. The Cartesian (x, y) and bipolar coordinates (ξ, η) are shown in figures 1 (*a*) and 1 (*b*), respectively.

Making use of vector identities and taking the curl of both sides of the resultant equation, the pressure is eliminated from (1) and one obtains

$$-\boldsymbol{\nabla}'\times(\boldsymbol{v}'\times\boldsymbol{\omega}')+\nu\boldsymbol{\nabla}'\times(\boldsymbol{\nabla}'\times\boldsymbol{\omega}')=\beta\boldsymbol{\nabla}'\times(\boldsymbol{g}(T_{\mathrm{w}}-T)), \tag{2}$$

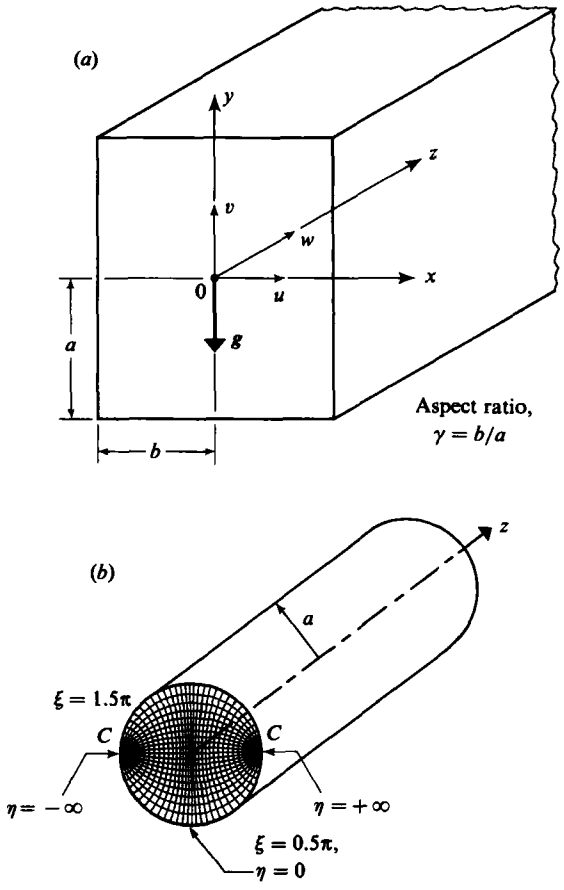

FIGURE 1 (*a*). Cartesian co-ordinate system for rectangular duct. (*b*). Bipolar co-ordinate system for the circular geometry duct.

where the vorticity vector is given by

$$\boldsymbol{\omega}' = \boldsymbol{\nabla}' \times \boldsymbol{v}'. \tag{3}$$

The z-direction of (2) gives the axial vorticity equation.

The equations of motion and energy for the fully developed mixed free and forced convection flow are given in dimensionless form as:

Stream function equation: $$\nabla^2 \psi = -\Omega. \tag{4}$$

Axial vorticity equation: $$\nabla^2 \Omega - (\boldsymbol{v} \cdot \boldsymbol{\nabla}) \Omega = B. \tag{5}$$

Axial velocity equation: $$\nabla^2 w - (\boldsymbol{v} \cdot \boldsymbol{\nabla} w) = -1. \tag{6}$$

Energy equation: $$\nabla^2 \phi - Pr\,(\boldsymbol{v} \cdot \boldsymbol{\nabla} \phi) = -\frac{w}{\langle w \rangle} \frac{1}{A}. \tag{7}$$

The condition of axially constant heat flux is reflected in the right-hand side of (7). The quantity A is given by

$$A = \text{flow area}/a^2,$$

where a is the radius for the bipolar coordinates or half-height of the rectangular duct for the Cartesian coordinates;

$$B = Gr\frac{\partial \phi}{\partial x} \quad \text{for the Cartesian coordinates}$$

$$B = -Gr\left[\sin\xi \sinh\eta \frac{\partial \phi}{\partial \xi} + (-1 + \cos\xi \cosh\eta)\frac{\partial \phi}{\partial \eta}\right] \quad \text{for the bipolar coordinates.}$$

Ω is the z-component of the dimensionless vorticity, w is the dimensionless axial velocity, ϕ is the dimensionless temperature, Pr is Prandtl number, Gr is Grashof number and γ is the rectangular duct aspect ratio, b/a. For the case of Cartesian coordinates (x, y):

$$\boldsymbol{v}\cdot\boldsymbol{\nabla} = u\frac{\partial}{\partial x} + v\frac{\partial}{\partial y}, \quad \nabla^2 = \frac{\partial^2}{\partial x^2} + \frac{\partial^2}{\partial y^2}, \tag{8a,b}$$

$$u = \frac{\partial \psi}{\partial y}, \quad v = -\frac{\partial \psi}{\partial x} \quad \text{and} \quad \Omega = \frac{\partial v}{\partial x} - \frac{\partial u}{\partial y} \tag{8c,d,e}$$

For the case of bipolar coordinates (ξ, η):

$$\nabla^2 = f_1^2\left[\frac{\partial^2}{\partial \xi^2} + \frac{\partial^2}{\partial \eta^2}\right], \quad \boldsymbol{v}\cdot\boldsymbol{\nabla} = f_1\left[v_\xi \frac{\partial}{\partial \xi} + v_\eta \frac{\partial}{\partial \eta}\right], \tag{9a,b}$$

$$f_1 = \cosh\eta - \cos\xi, \quad v_\xi = -f_1\frac{\partial \psi}{\partial \eta}, \tag{9c,d}$$

$$v_\eta = f_1\frac{\partial \psi}{\partial \xi} \quad \text{and} \quad \Omega = -f_1\left[\frac{\partial v_\eta}{\partial \xi} - \frac{\partial v_\xi}{\partial \eta}\right] + v_\eta \sin\xi - v_\xi \sinh\eta. \tag{9e,f}$$

The flow and energy equations are rendered dimensionless as follows:

$$\psi = \psi'/\nu, \quad \Omega = \Omega'/(\nu/a^2),$$

$$w = \frac{w'}{-\dfrac{\mathrm{d}p^*}{\mathrm{d}z'}(a^2/\mu)}, \quad x = x'/a, \quad y = y'/a,$$

$$z = z'/a, \quad \phi = \frac{T_w - T}{Q'/k} \quad \text{and} \quad Gr = \frac{Q' g\beta a^3}{k\nu^2}.$$

The secondary velocities were rendered dimensionless using (ν/a); k is the fluid thermal conductivity, ν is the fluid kinematic viscosity and Q' is the heat flux per unit length of the duct. The term $\mathrm{d}p^*/\mathrm{d}z'$ is the axial pressure gradient and it is constant for a fully developed flow. For the case of the bipolar coordinates, the transformation

$$\eta = \tfrac{1}{2}(\mathrm{e}^\beta - 1)$$

has been found to be useful in providing more grid points near the coordinate $\eta = 0$. The boundary conditions are:

$\psi = w = \phi = 0$ along the duct walls;

$\Omega = \psi = \dfrac{\partial w}{\partial x} = \dfrac{\partial \phi}{\partial x} = 0$ along $x = 0$ for Cartesian coordinates;

$\Omega = \psi = \dfrac{\partial w}{\partial \eta} = \dfrac{\partial \phi}{\partial \eta} = 0$ along $\eta = 0$ for bipolar coordinates;

$$\left.\begin{aligned} \Omega &= -\frac{\partial^2\psi}{\partial x^2} \quad \text{along constant } x \\ \Omega &= -\frac{\partial^2\psi}{\partial y^2} \quad \text{along constant } y \end{aligned}\right\} \text{for Cartesian coordinates;}$$

$$\left.\begin{aligned} \Omega &= -f_1^2\frac{\partial^2\psi}{\partial \xi^2} \quad \text{along constant } \xi \\ \Omega &= -f_1^2\frac{\partial^2\psi}{\partial \eta^2} \quad \text{along constant } \eta \end{aligned}\right\} \text{for bipolar coordinates.}$$

The macroscopic quantities are given by

$$f\,Re = \frac{2\,De\,A}{P\langle w\rangle}, \tag{10}$$

where the Reynolds number $Re = De'\langle w'\rangle/\nu$, f is the Fanning friction factor, A is the flow area dimensionalized with a^2, P is the wetted perimeter dimensionalized using a and De is the dimensionless equivalent diameter ($De = De'/a$), and $De' = 4$ flow area/wetted perimeter.

The average Nusselt number, based on the equivalent diameter, is given by

$$Nu = \frac{De}{P}\frac{1}{\phi_b}, \tag{11}$$

where ϕ_b is the mixing-cup fluid temperature defined as

$$\phi_b = \int_A w\phi\,\mathrm{d}A \Big/ \int_A w\,\mathrm{d}A. \tag{12}$$

3. Method and accuracy of solution

The governing partial differential equations were discretized using central difference approximations. As both diffusive and convective mechanisms are important in this problem, central-difference approximations were preferred over the upwind differencing scheme, as the latter might introduce parasitic effects and false scaling as shown by Strikwerda (1982). The resulting algebraic equations were solved using a successive relaxation method. The equations were solved in the order of ϕ–Ω–ψ–w until convergence was attained. For the rectangular duct most of the solutions were obtained using a uniform grid of 21×21 over the domain $0 < x < \gamma$ and $-1 < y < 1$. The adequacy of this grid size in providing accurate solutions was tested by reproducing established solutions for the limiting case of forced convection (i.e. $Gr = 0$). The computed results shown in table 1, for different aspect ratios, agree within 1 % of published values in all cases. Next, the results of Cheng & Hwang (1969) were reproduced for the mixed convection problem for Grashof numbers of up to 50000. The flow and heat-transfer results for this case are shown in figures 2 and 3 respectively. Next, the grid resolution was increased from 21×21 to 21×41 for the two cases of $Gr = 100000$ (with the two-vortex pattern) and $Gr = 500000$ (with a four-vortex pattern). In the first case the $f\,Re$ and Nu changed from 20.230 and 6.194 to 20.219 and 6.203, respectively. In the second case the changes were from 27.046 and 8.898 to 27.014 and 8.879, respectively. The 21×21 grid was found to be adequate for predicting both the two- and four-vortex patterns over the aspect-ratio range of

Duct type	Aspect ratio	Literature values Shah & London (1978) fRe	Literature values Shah & London (1978) Nu	This work fRe	This work Nu	Grid
Rectangular	1.0	14.227	3.608	14.247	3.597	21 × 21
Rectangular	2.0	15.548	4.123	15.565	4.115	21 × 21
Circular	—	16	4.364	16.027	4.317	21 × 31
Semi-circular	—	15.767	4.089	15.788	4.053	21 × 21

TABLE 1

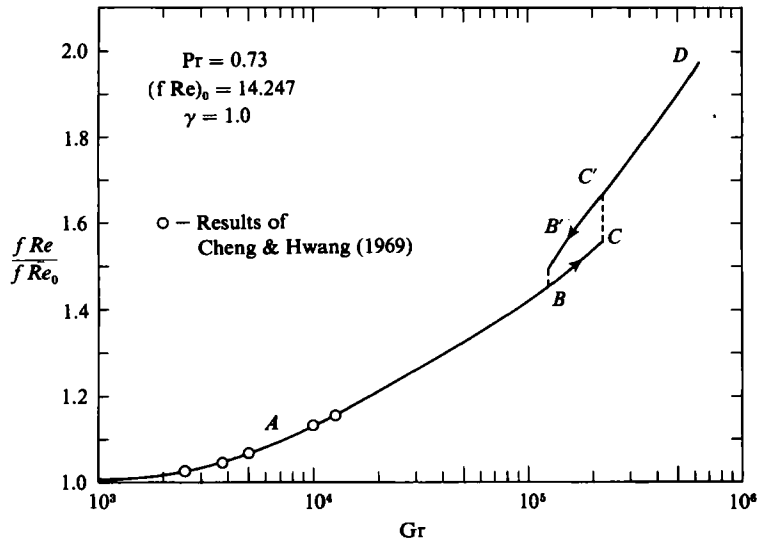

FIGURE 2. Friction-factor variation with Grashof number showing hysteresis behaviour for rectangular duct (axially uniform flux, peripherally uniform temperature).

0.7 to 1.5 and for Grashof numbers of up to 800000. Clearly, as the aspect-ratio is increased to much larger values, the flow undergoes a series of transitions giving rise to a multicellular flow pattern. In such cases the grid resolution in the x-direction has to be increased significantly. This problem was addressed recently by Lee & Korpela (1983) for a purely natural convection flow in long vertical enclosures. They found that 10 grid points per cell were adequate. Similar tests were conducted for the case of circular and semicircular ducts. Table 1 shows results for $Gr = 0$. The agreement is again within 1 % of the published data. We believe that the macroscopic results presented in this study are accurate to better than 2 %.

4. Results

4.1. *Rectangular ducts*

First, we re-examine the problem studied by Cheng & Hwang (1969). Their results are extended for Grashof numbers of up to 600000. The friction-factor and Nusselt number results are presented in figures 2 and 3, respectively, for an aspect ratio of 1 and $Pr = 0.73$. The friction-factor and Nusselt number data show a hysteresis

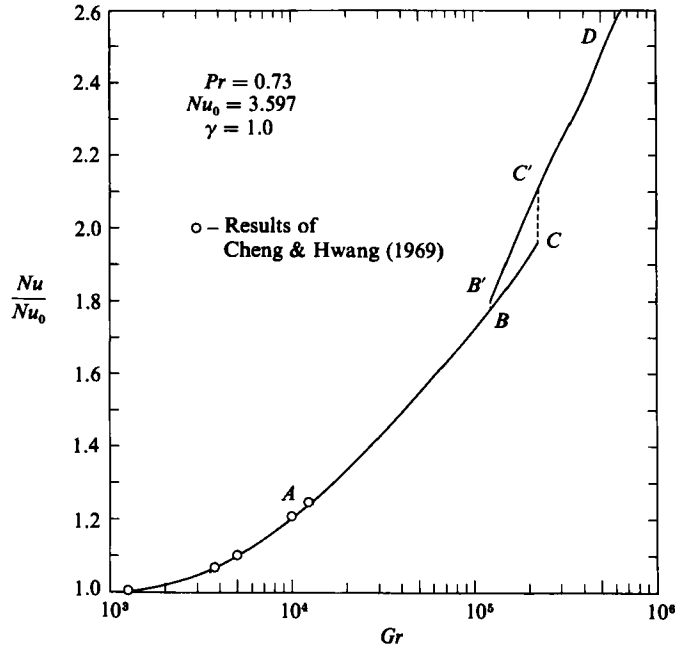

FIGURE 3. Nusselt number variation with Grashof number for rectangular duct (axially uniform flux, periplurally uniform temperature).

behaviour as the Gr number is *gradually* increased and then decreased. For $Gr > 225000$ only a four-vortex solution is present while for $Gr < 125000$ only a two-vortex solution is present. Between these two limits, both types of solutions are possible. The bifurcation set of critical points for the two- to four-vortex transition is new.

It is of interest to give the detailed manner by which the results of figures 2 and 3 were obtained. Starting with a converged solution for a small Gr, say 1000, as the initial guess of the field, a converged solution was then obtained for a slightly higher Gr value, say 5000. Making use of the converged solution at $Gr = 5000$, a new solution was obtained at a slightly higher Gr. In this manner data points along ABC were obtained and the solution exhibited a two-vortex flow pattern. On further increasing Gr beyond point C, the solution exhibited a four-vortex flow pattern along $C'D$. On gradually decreasing Grashof number along DC' it was possible to maintain the four-vortex solution till point B'. On further decreasing Gr beyond BB' the two-vortex solution is recovered in a catastrophic manner. Thus a hysteresis behaviour is present for this type of flow.

When there are two truly varying parameters such as a lengthscale of a geometry and a flow parameter, and two possible modes of behaviour such as a two- and a four-vortex flow pattern, this phenomenon can be interpreted in terms of a cusp catastrophe as was done by Benjamin (1978*a*, *b*) in his experiments on the Taylor problem with a finite geometry.

The critical Grashof number variation with the duct aspect ratio is shown in figure 4. For an aspect ratio of unity, the critical points (B, B') and (C, C') of figures 2 and 3 are shown on figure 4. The curve of figure 4 was established using the method of bisection. The length of the arrows indicates the uncertainty in the location of the critical points. This curve was established using about 300 simulation runs. Both the

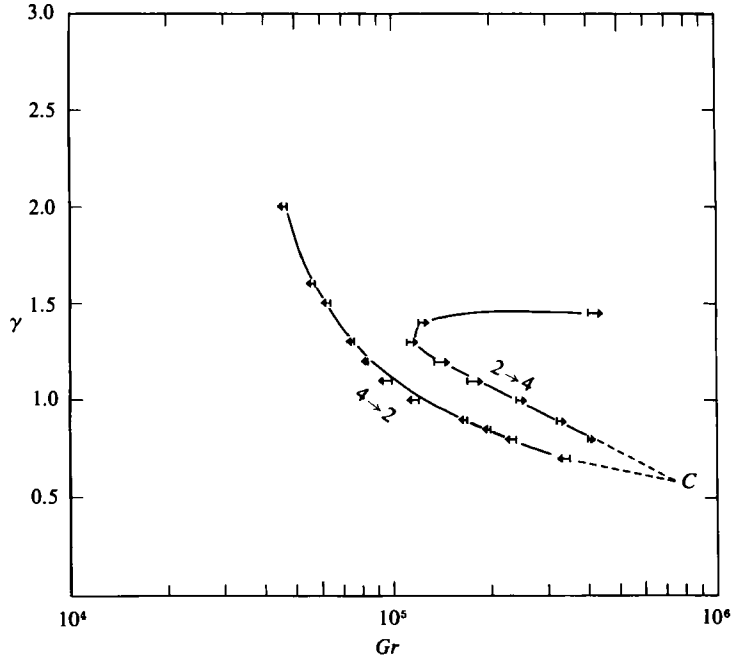

FIGURE 4. Critical Grashof number variation with aspect ratio.

upper ($2 \rightarrow 4$) and lower ($4 \rightarrow 2$) critical Gr numbers are shown as a function of aspect ratio over the range of 0.7–2. As the aspect ratio is decreased below unity, both critical points increase quite rapidly. It was extremely difficult to locate the critical points for aspect ratios lower than 0.7 as the numerical method failed at large Gr numbers. Hence, the critical curves are extrapolated by dotted lines in this region. This figure has a strong resemblance to the tilted cusp observed by Benjamin in his experiments on Taylor vortices. With the friction factor as the state function and the aspect ratio and Gr number as the control parameters, one would obtain the folded surface that is typical of cusp catastrophe and figure 4 maps the boundaries of the fold on such a surface.

Contours of the axial velocity w, temperature ϕ and stream function ψ are shown in figure 5. The effect of the buoyancy force is to shift the point of maximum axial velocity in the direction of the body force resulting in a steep velocity gradient near that wall. This is indicative of a boundary-layer structure close to the lower wall. In a theoretical study by Mori & Futagami (1967), such a flow structure has been imposed *a priori* on the equations in order to effect a solution at high Grashof numbers. Such approximations, however, inhibit the unfolding of the four-vortex pattern, which is inconsistent with a model of inviscid core and a boundary layer near the wall. This is evident from the contours of the flow field shown for the four-vortex pattern at Grashof numbers of 200000 and 500000. The values of the contours of the stream function indicate that the flow reversal is quite intense in the vortices close to the lower duct wall.

The effect of aspect ratio on the qualitative nature of the secondary flow is shown in figure 6. The stream-function contours are shown for the four-vortex pattern only, over the aspect-ratio range of 0.8–4.4. As the aspect ratio is increased, the Grashof number had to be decreased gradually in order to obtain a stable converged solution.

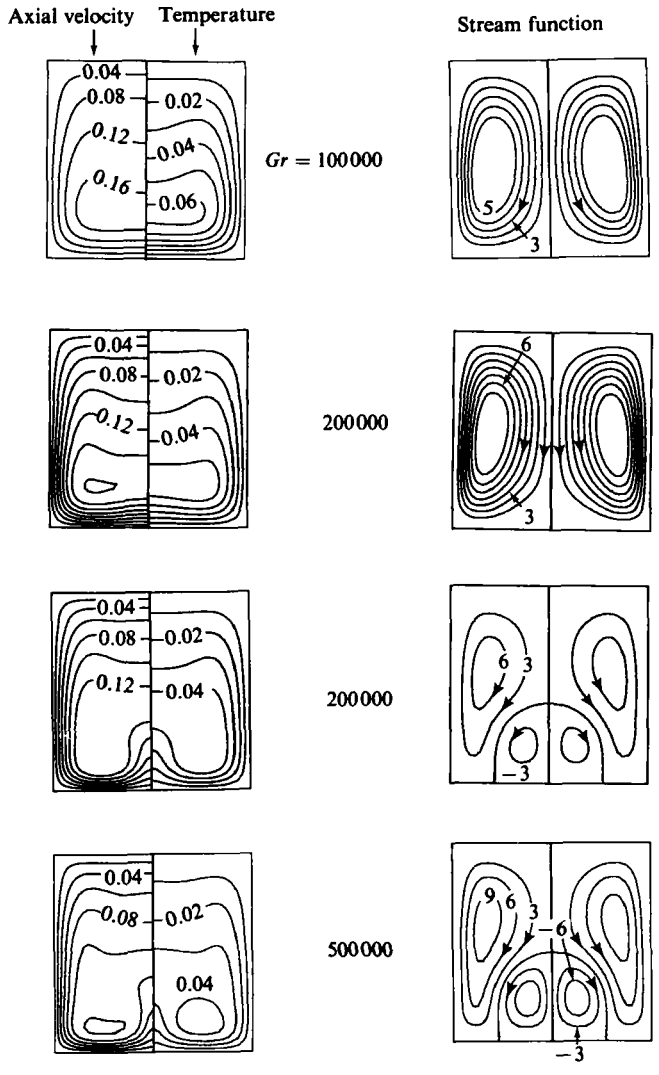

FIGURE 5. Contours of axial velocity, temperature and stream function for rectangular duct.

For a small aspect ratio, the size of the secondary vortex is small and it appears only at a fairly high Grashof number. As the aspect ratio is increased the size, as well as the strength, of the secondary vortex increases and it appears more readily at lower Gr numbers. On further increase in aspect ratio, the separation point on the line of symmetry moves towards the top of the tube (figure 6*f*) and then moves along the top of the tube and away from the line of symmetry. For a particular choice of aspect ratio that is consistent with a characteristic length of the cells, one would expect the streamline separating the vortices to become vertical. Furthermore, it appears that the size of the two central vortices will be smaller than the two end vortices and this is attributed to the boundary effect on the end cells.

One can then begin to see, in figure 6, the origin of the multicellular flow pattern. Starting with low values of aspect ratio, the transition from a two- to a four-vortex pattern occurs abruptly, i.e. through a bifurcation. The secondary vortices appear

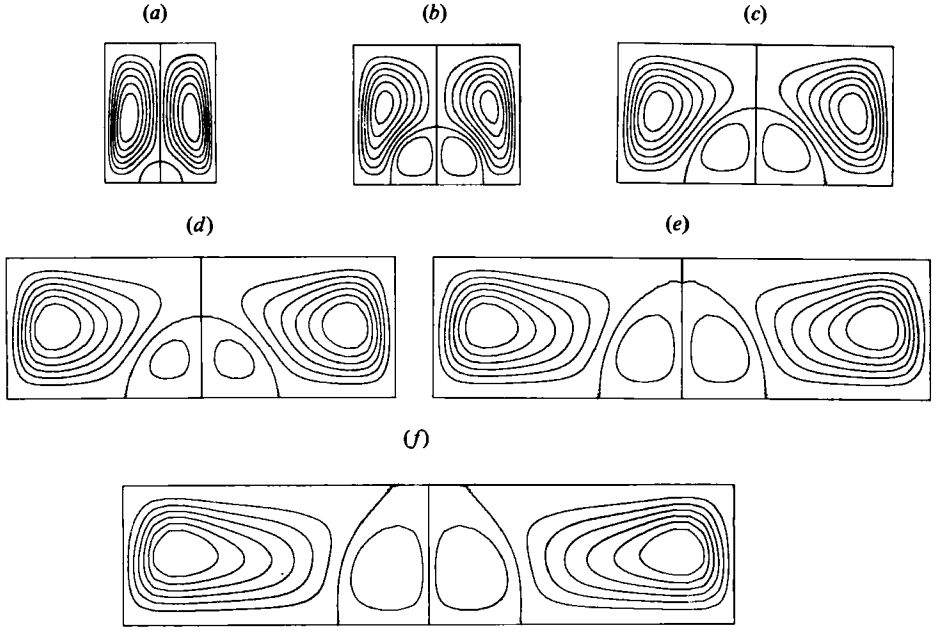

FIGURE 6. Flow pattern for the rectangular duct with different aspect ratio stream function contours: (*a*) $Gr = 160000$, $Pr = 0.73$, $AR = 0.8$; (*b*) 100000, 0.73, 1.2; (*c*) 50000, 0.73, 2.0; (*d*) 40000, 0.73, 2.8; (*e*) 30000, 0.73, 3.6; (*f*) 50000, 0.73, 4.4.

at the lower side (i.e. the side facing the body force) and are small in size. As the aspect ratio is increased, they grow in size and strength until they become comparable to the primary vortices. At this stage, the primary flow (or mode) itself is deemed to consist of four vortices. With further increase in aspect ratio, two more new secondary vortices would appear at the lower plate through a bifurcation. They, in turn, would grow in size until they become indistinguishable from the neighbouring vortices. The end vortices would, of course, be different due to end boundary conditions. Hence, in the parameter space of aspect ratio and Grashof number, the multicellular pattern appears to emerge through a series of bifurcation processes when viewed in the direction of increasing aspect ratio, provided the Gr number is above a certain threshold value.

The velocity component in the y direction along the centreline ($x = 0$) is shown in figure 7 for Gr numbers of 100000, 200000 and 500000. The velocity in the smaller vortex (secondary) is seen to be much stronger than in the primary vortex, indicating that the circulation in the secondary vortex is fairly intense. For $Gr = 500000$ the flow reversal occurs at $x = 0$, $y = -0.1$. From figure 5, the stream-function contour separating the two vortices passes through this point and intersects the line of symmetry at right angles. The axial velocity and temperature profiles along the two perpendicular lines through this point of separation are shown in figure 8. Along the line of symmetry, both profiles show a fairly strong maximum at the point of separation. Along the $y = -0.1$ line, both the profiles are essentially flat in the central core with sharp gradients near the boundary. At the point of separation, the axial velocity exhibits a very weak local minimum. This is not an aberration due to the numerical scheme as it is preserved with grid refinement (21×21 to 21×41). The flow

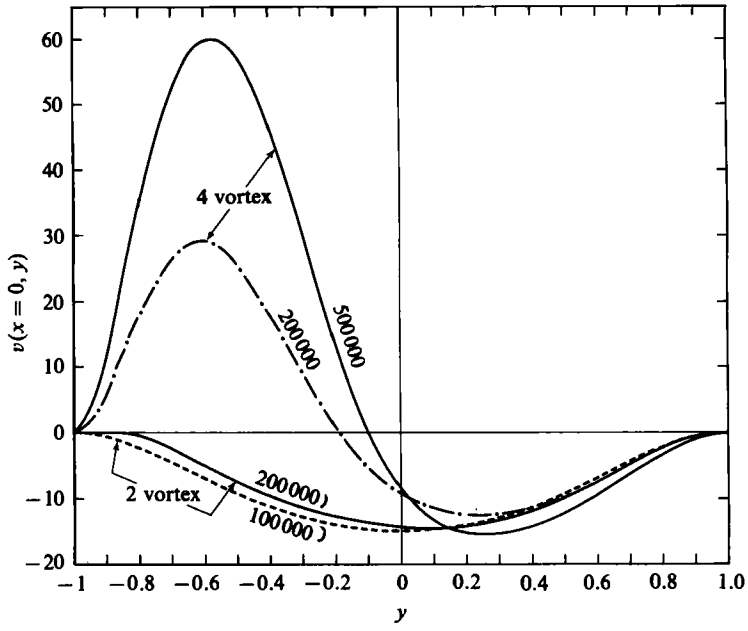

FIGURE 7. The y-component velocity variation for the rectangular duct.

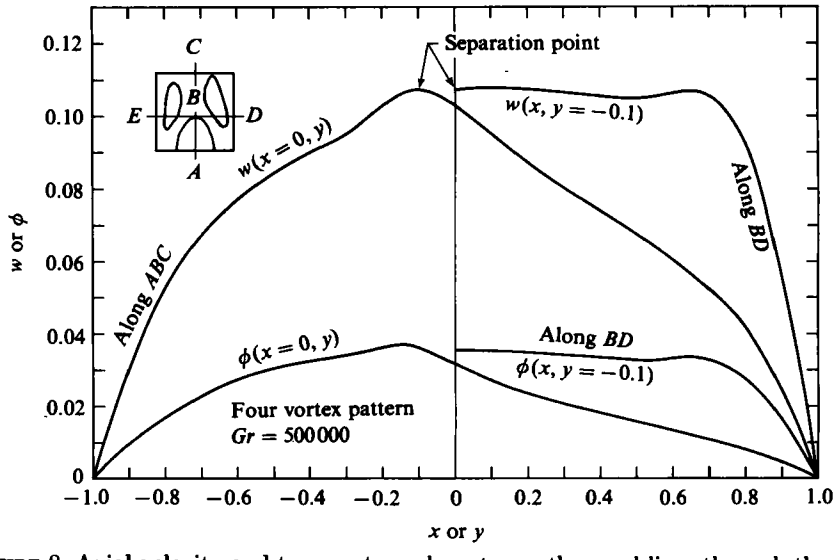

FIGURE 8. Axial velocity and temperature along two orthogonal lines through the separation point illustrating the saddle point at B for the rectangular duct.

characteristics near the separation point are similar to flow through helical tubes (Nandakumar & Masliyah 1982).

It is apparent from the results presented here that there is a strong similarity between the mixed convection flow in a straight duct and the isothermal flow in a helical duct, Dean problem. In the flow through a helical duct, it is the centrifugal

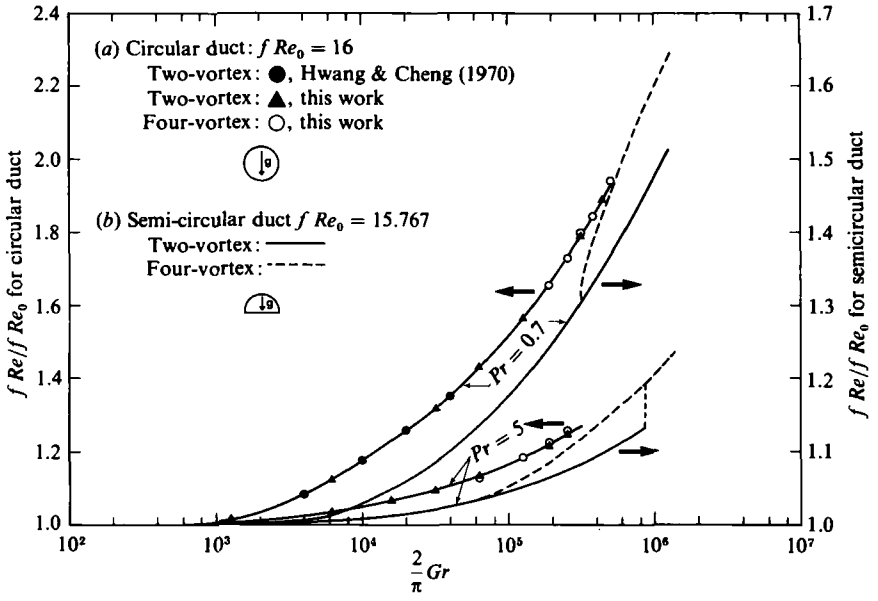

FIGURE 9. Friction-factor variation with Grashof number for circular and semicircular ducts.

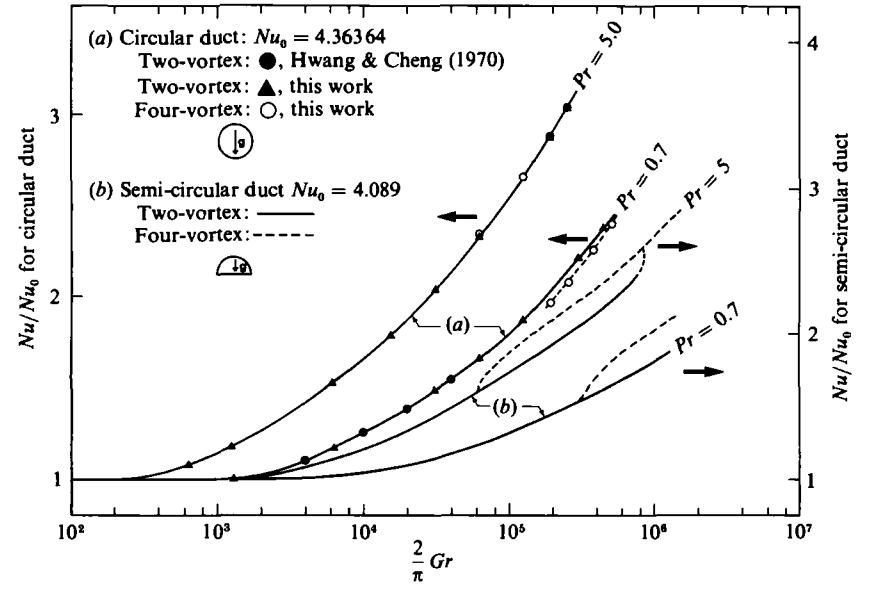

FIGURE 10. Nusselt number variation with Grashof number for circular and semicircular ducts.

force due to the axial velocity that drives the secondary flow. The axial velocity and stream-function contours of figure 5, the secondary velocity v of figure 7 and the axial velocity of figure 8 are very similar to those presented by Nandakumar & Masliyah (1982) for the case of isothermal flow in a helical duct. It should be noted here that the stream function and the axial velocity equations for the flow in a helical duct, subject to the loose coiling approximation, are the same as those for mixed free and

forced convection flow and that the axial vorticity equation is different in the form of the forcing function only. Thus the similarity between the two flow problems is not surprising.

4.2. *Circular and semicircular ducts*

The friction-factor and Nusselt number variations with Grashof number are shown in figures 9 and 10, respectively. The results for the two-vortex solution for the circular duct are in agreement with those of Hwang & Cheng (1970). Dual solutions are present above a critical Grashof number for both the circular and the semicircular ducts at $Pr = 0.7$ and 5.0. For the case of a circular geometry, the two- and four-vortex solutions showed little difference in the values of fRe and Nu. For the case of a semicircular duct, the four-vortex solution gave values of fRe and Nu significantly different to those for the two-vortex solution. This appears to be a characteristic feature of a geometry with a flat wall facing the body force vector, as this behaviour was also observed in laminar flow through helical tubes (Nandakumar & Masliyah 1982). For convenience, this reference subsequently will be referred to as (I).

For the circular duct at $Pr = 0.7$ and 5 and for the semicircular duct at $Pr = 0.7$, only the lower critical Grashof number could be found, i.e. the transition from four- to two-vortex solution. However, for the case of a semicircular duct at $Pr = 5$ both values of the critical Grashof numbers were established. For the latter case, the plots of fRe and Nu can be obtained by gradually increasing the Grashof number and subsequently decreasing its value as for the case of the rectangular ducts. However, for the other cases, the upper critical Grashof number could not be reached due to the instability of the numerical scheme at high Grashof numbers.

In our study we initially fixed Pr at a value of 0.73. As the upper critical Grashof number could not be reached for this case, the four-vortex solution could not be established as the primary flow. It nevertheless exists as a secondary mode in the range of dual solutions, i.e. between the lower and upper critical Grashof numbers. Consequently in order to obtain the four-vortex solution as a secondary mode some 'trick' had to be employed. Had we initially solved for $Pr = 5$ for the semicircular duct, we would have then obtained the four-vortex solution once the upper critical Grashof number was exceeded. We would have then used the four-vortex solution as the initial guess for a $Pr = 0.73$ case in order to generate a four-vortex solution. In order to obtain a four-vortex solution for a $Pr = 0.73$ we used the analogy between the Dean problem and the mixed-convection problem to establish the four-vortex solution for the latter. A converged four-vortex solution that we had obtained as in (I) was transformed and rescaled appropriately for the mixed-convection problem and was used as the *initial* guess for the iterative solution procedure. Once a four-vortex pattern was established this way, it was then sustained quite readily for other cases by making small changes in Gr, Pr or the geometrical parameter.

The contours of axial velocity, temperature and stream function are shown in figure 11 for the case of $Gr = 600000$ and $Pr = 0.7$. Both the two- and four-vortex patterns are evident at the same operating conditions. There is a striking similarity between the contours of axial velocity and temperature as well as a similarity between the axial velocity for this problem and the Dean problem (see I). When like profiles of axial velocity and temperature drive the secondary flow, one can expect similar secondary-flow patterns for curved flow and buoyancy-induced flow. The stream function contours confirm this expectation. For the four-vortex pattern, the point of separation along the line of symmetry appears to be a saddle point for axial velocity, very much like that of the Dean problem, (I).

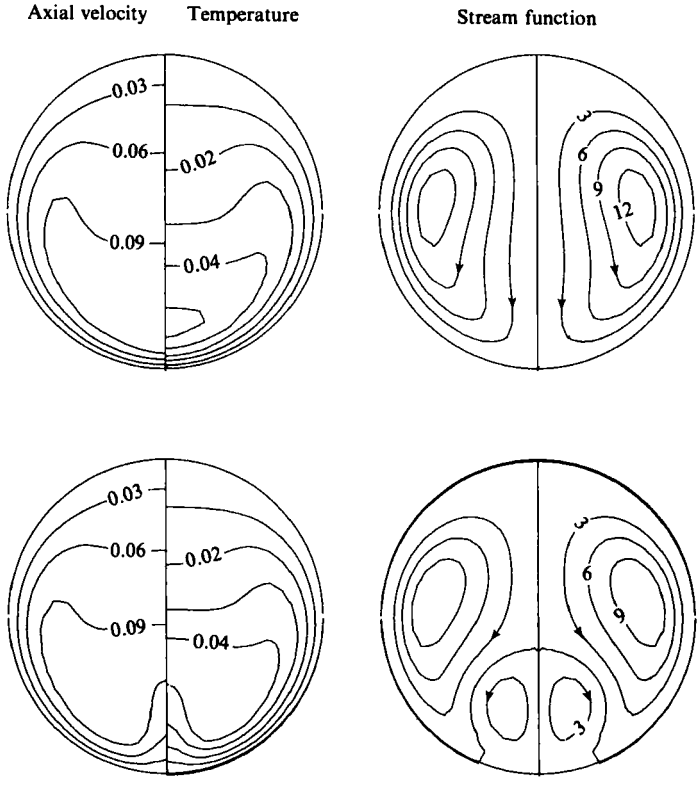

FIGURE 11. Contours of flow and temperature for $Gr = 600000$ and $Pr = 0.7$.

A similar portrait of contours is shown in figure 12 for a semicircular geometry with a flat bottom wall for a Pr number of 0.7 and 5.0. For both geometries the strength of the secondary flow is weakened considerably with an increase in Prandtl number. This is due to an almost flat temperature profile in the core region, which provides a weak driving force for the secondary flow. However, dual solutions are present for both cases.

In the earlier study (I) we examined the Dean problem in helical ducts along the same lines as in this study. The shape of the outer surface of the duct was determined by one of the coordinate lines, ξ_0. It was changed from a full circle to a semicircle through several moon-shaped configurations. Then the effect of ξ_0 and Dn on flow pattern changes was examined. The critical Dean number was insensitive to changes in ξ_0. This is in contrast to a rectangular geometry where the critical flow parameter (Taylor, Grashof or Dean number) is a strong function of the geometrical parameter, i.e. aspect ratio. This is because changes in ξ_0 for a circular geometry do not change the lengthscale significantly. Hence, we are left with only one effective control parameter, *viz* the flow parameter, Grashof number or Dean number. This should then yield only a fold catastrophe with a lower and upper critical flow parameter. In our numerical experiments in (I) we observed only the lower critical Dean number and a duality of solutions above that number. We believe that there is an upper critical Dean number above which only a four-vortex solution is possible. But the numerical method used to solve the Dean problem failed before the upper critical Dean number could be reached. While we encountered similar difficulties with the

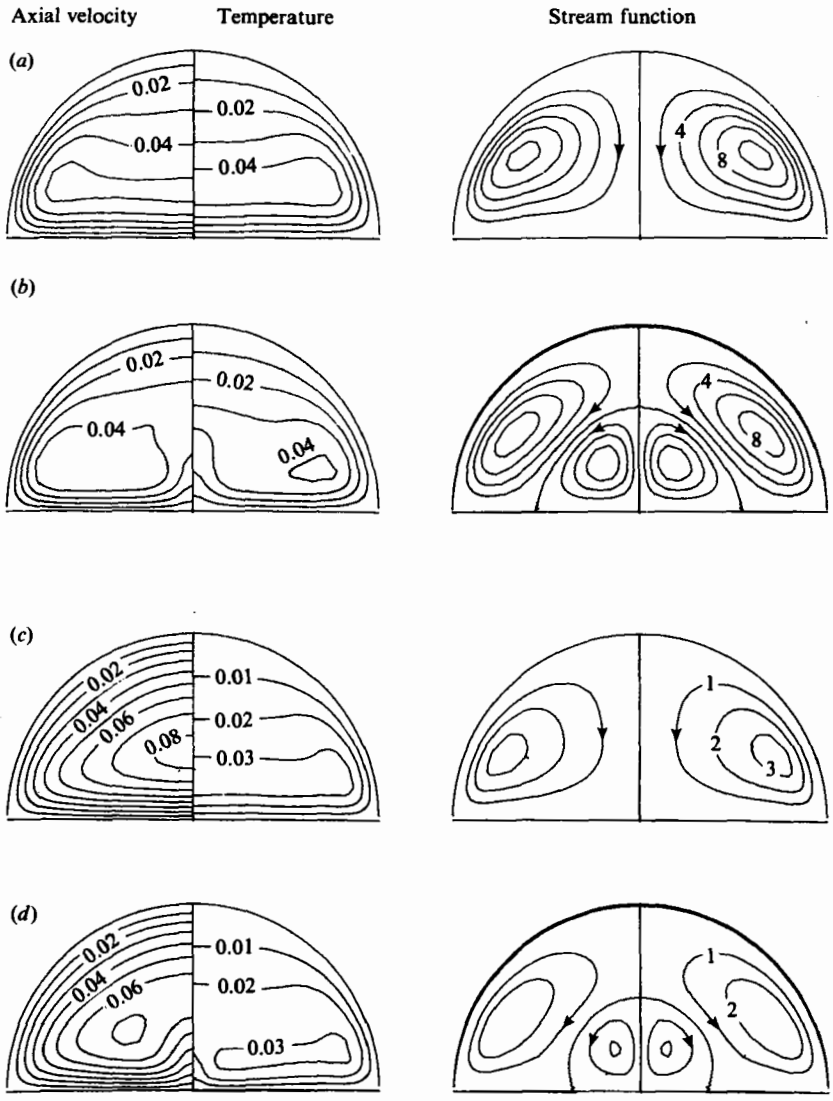

FIGURE 12. Contours of flow and temperature for semicircular ducts: (*a*) and (*b*) $Gr = 1.6 \times 10^6$, $Pr = 0.7$; (*c*) and (*d*) $Gr = 1.2 \times 10^6$, $Pr = 5.0$.

mixed convection problem in this work, at least one case (a semicircle with $Pr = 5$) indicates that there is a lower and an upper critical Grashof number for this problem. In the other cases we find only the lower critical Grashof number.

5. Conclusions

The mixed-convection flow problem in horizontal rectangular, circular and semicircular ducts subject to axially uniform flux and peripherally uniform temperature was shown to exhibit flow bifurcation. In particular, for the case of the rectangular duct, flow hysteresis was shown to be present. Similarity between the mixed-convection flow problem and the Dean problem is shown to be fairly strong.

The authors wish to thank the National Science and Engineering Research Council of Canada for the financial support.

REFERENCES

BENJAMIN, T. B. 1978*a* Bifurcation phenomena in steady flows of a viscous fluid. I. Theory. *Proc. R. Soc. Lond.* A **359**, 1–26.

BENJAMIN, T. B. 1978*b* Bifurcation phenomena in steady flows of a viscous fluid. II. Experiments. *Proc. R. Soc. Lond.* A **359**, 27–43.

BENJAMIN, T. B. & MULLIN, T. 1981 Anomalous modes in the Taylor experiment. *Proc. R. Soc. Lond.* A **377**, 221–249.

BENJAMIN, T. B. & MULLIN, T. 1982 Notes on the multiplicity of flows in the Taylor experiment. *J. Fluid Mech.* **121**, 219–230.

BERGLES, A. E. & SIMONDS, R. R. 1971 Combined forced and free convection for laminar flow in horizontal tubes with uniform heat flux. *Intl J. Heat Mass Transfer* **14**, 1989–2000.

CHENG, K. C. & HWANG, G.-J. 1969 Numerical solution for combined free and forced laminar convection in horizontal rectangular channels. *Trans. ASME* C: *J. Heat Transfer* **91**, 59–66.

CHENG, K. C., NAKAYAMA, J. & AKIYAMA, M. 1977 Effect of finite and infinite aspect ratios on flow patterns in curved rectangular channels. *Int. Symp. on Flow Visualization, Tokyo, Oct. 1977*, 109–114.

CLIFFE, K. A. 1983 Numerical calculations of two-cell and single-cell Taylor flows. *J. Fluid Mech.* **135**, 219–233.

DENNIS, S. C. R. & NG, M. 1982 Dual solutions for steady laminar flow through a curved tube. *Q. J. Mech. Appl. Maths* **35**, 305–324.

FARIS, G. N. & VISKANTA, R. 1969 An analysis of combined forced and free convection heat transfer in a horizontal tube. *Intl. J. Heat Mass Transfer* **12**, 1295–1309.

HWANG, G. J. & CHENG, K. C. 1970 Boundary vorticity method for convective heat transfer with secondary flow – applications to the combined free and forced laminar convection in horizontal tubes. *Heat Transfer* **4**, Paper no. NC3.5.

IQBAL, M. & STACHIEWICZ, J. W. 1966 Influence of tube orientation on combined free and forced laminar convection heat transfer. *Trans. ASME C*: *J. Heat Transfer* **88**, 109–116.

IQBAL, M. & STACHIEWICZ, J. W. 1967 Variable density effects in combined free and forced convection in inclined tubes. *Intl J. Heat Mass Transfer* **10**, 1625–1629.

JALURIA, Y. 1980 *Natural Convection Heat and Mass Transfer*. Pergamon.

KATO, K., WATANABE, E., OGURA, T. & HANZAWA, T. 1982 Effect of natural convection on laminar flow heat transfer in horizontal circular tubes. *J. Chem. Enging of Japan* **15**, 335–361.

KELLER, H. B. 1977 *Numerical Solutions of Bifurcation and Nonlinear Eigenvalue Problems; Applications of Bifurcation Theory* (ed. P. H. Rabinowitz), pp. 359–384. Academic.

LEE, Y. & KORPELA, S. A. 1983 Multicellular natural convection in a vertical slot. *J. Fluid Mech.* **126**, 91–121.

MASLIYAH, J. H. 1980 On laminar flow in curved semicircular ducts. *J. Fluid Mech.* **99**, 469–479.

MCCOMAS, S. T. & ECKERT, E. R. G. 1966 Combined free and forced convection in horizontal circular tubes. *Trans. ASME C*: *J. Heat Transfer* **88**, 147–153.

MORI, Y. FUTAGAMI, K., TOKUDA, S. & NAKAMURA, M. 1966 Forced convective heat transfer in uniformly heated horizontal tubes (1st Report: experimental study on the effect of buoyancy). *Int. J. Heat Mass Transfer* **9**, 453–463.

MORI, Y. & FUTAGAMI, K. 1967 Forced convective heat transfer in uniformly heated horizontal tubes (2nd Report; Theoretical Study). *Intl J. Heat Mass Transfer* **10**, 1801–1813.

MORTON, B. R. 1959 Laminar convection in uniformly heated horizontal pipes at low Rayleigh numbers. *Q. J. Mech. Appl. Maths* **12**, 410–420.

MULLIN, T. 1982 Mutations of steady cellular flows in the Taylor experiment. *J. Fluid Mech.* **121**, 207–218.

NANDAKUMAR, K. & MASLIYAH, J. H. 1982 Bifurcation in steady laminar flow through curved tubes. *J. Fluid Mech.* **119**, 475–490.

NANDAKUMAR, K. & MASLIYAH, J. H. 1984 Review of swirling flow and heat transfer in coiled and twisted pipes. To appear in *Advances in Transport Processes* (ed. A. S. Mujumdar & R. A. Mashelkar). Wiley Eastern Ltd.

NEWELL, P. H. & BERGLES, A. E. 1970 Analysis of combined free and forced convection for fully developed laminar flow in horizontal tubes. *Trans. ASME C: J. Heat Transfer* **90**, 83–93.

PATANKAR, S. V., RAMADHYANI, S. & SPARROW, E. M. 1978 Effect of circumferentially nonuniform heating on laminar combined convection in a horizontal tube, *Trans. ASME C: J. Heat Transfer* **100**, 63–70.

SHAH, R. K. & LONDON, A. L. 1978 *Laminar Flow Forced Convection in Ducts*. Academic.

SHANNON, R. L. & DEPEW, C. A. 1968 Combined free and forced convection in a horizontal tube with uniform heat flux. *Trans ASME C: J. Heat Transfer* **90**, 353–357.

STRIKWERDA, J. C. 1982 Upwind differencing, false scaling and nonphysical solutions to the driven cavity problem. *J. Comp. Phys.* **47**, 303–307.